Mitigation of magneto-Rayleigh-Taylor instability growth in a triple-nozzle, neutron-producing gas-puff Z pinch

J. Narkis [1,*] F. Conti [1] A. L. Velikovich,[2] and F. N. Beg[1]

[1]*Center for Energy Research, University of California San Diego, La Jolla, California 92093, USA*
[2]*Plasma Physics Division, Naval Research Laboratory, Washington, District of Columbia 20375, USA*

The gas-puff Z-pinch is a well-known source of x-rays and/or neutrons, but it is highly susceptible to the magneto-Rayleigh-Taylor instability (MRTI). Approaches to MRTI mitigation include density profile tailoring, in which nozzles are added or modified to alter the acceleration trajectory, and axial pre-magnetization, in which perturbations are smoothed out via magnetic field line tension. Here, we present two-dimensional magnetohydrodynamic simulations of loads driven by an 850 kA, 160 ns driver that suggest these mitigation strategies can be additive. The initial axial magnetic field, B_{z0}, to stabilize a 2.5-cm-radius Ne gas liner imploding onto an on-axis deuterium target can be reduced from 0.7 T to 0.3 T by adding a second liner with a radius of 1.25 cm. Because MRTI mitigation tends to increasingly lower yield with higher B_{z0}, the use of a lower field is advantageous. Here, we predict a reduction in yield penalty from $>100\times$ with the single liner to $<10\times$ with a double liner. A premagnetized, triple nozzle gas puff could therefore be an attractive source for intense neutrons or other fusion applications.

The gas-puff Z-pinch is an efficient method for producing x-rays or neutrons, in which an axial current applied to a cylindrical or annular gas shell induces an azimuthal magnetic field and the resulting force compresses the load radially [1–3]. Implosion timescales are typically matched to the current rise times of the pulsed power driver, with timescales of order 0.1–$1.0\,\mu$s and lengthscales of order 0.1–10 cm. The rapid acceleration of the shell to tens or hundreds of km/s makes the load highly susceptible to the magneto-Rayleigh-Taylor instability (MRTI) [4], in which the vacuum magnetic field serves as the "lighter fluid." Extensive analytical [5–13] and experimental [14–23] work on MRTI growth and mitigation in Z pinches has been conducted and remains an active area of research. In its simplest form (a Cartesian slab of constant density), the growth rate is

$$\gamma_{\mathrm{MRT}}^2 = gk - \frac{(\mathbf{k}\cdot\mathbf{B})^2}{\mu_0 m_i n_i}, \qquad (1)$$

where g is acceleration, $\mathbf{k}$ is the instability wave number, $\mathbf{B}$ is the magnetic field, μ_0 is the vacuum permeability, and m_i and n_i are ion mass and number density, respectively. The embedding of an axial magnetic field, as will be done here, will only mitigate MRTI growth of the azimuthally symmetric modes, i.e., $\mathbf{k}\cdot\mathbf{B} \equiv k_z B_z$; hence the present discussion will be correspondingly restricted. There is some evidence that three-dimensional (3-D) modes can develop [22,24] and that they may be driven by extended magnetohydrodynamic (MHD) effects such as the Hall effect [12,20]. However, this is beyond the scope of this work and left to future study.

For any potential gas-puff configuration that uses a pre-embedded axial magnetic field B_{z0} for MRTI mitigation, it is of interest to establish a minimum B_{z0} such that MRTI growth does not disrupt the implosion. Generally speaking, this is because there is a tradeoff between pinch stability and maximum attainable thermonuclear neutron yield. Although unstable pinches may locally reach high convergence, creating hot spots that produce the majority of the thermonuclear yield, without any instability mitigation they may not do so reliably, which could limit their usefulness in future applications such as fusion [25,26] that require reproducibility. On the other hand, if the pinch is stabilized with a large B_{z0}, the fuel column may on average be tighter and more uniform, but by suppressing the formation of hot spots, the overall yield may decrease.

The ideal MHD stability analysis of Ref. [5] estimated that a single-shell implosion is stabilized by a field approximately given by

$$B_{st}\,[\mathrm{T}] = \frac{I_{pk}\,[\mathrm{MA}]}{R_0\,[\mathrm{cm}]}, \qquad (2)$$

where I_{pk} is the driver peak current and R_0 is the initial pinch radius. A field of $\sim 0.5 B_{st}$ has been shown empirically to stabilize single shell-on-target implosions, and, to some degree, even hollow shell implosions [15]. The recent results of the authors of Ref. [22] suggest some degree of stabilization even at values of $B_{z0} = 0.1\,\mathrm{T}$ in a 1.3-cm implosion on a 1-MA driver, or $0.13 B_{st}$. Despite the abundance of experimental study and one-dimensional (1-D) MHD simulations, the problem has yet to be studied numerically in two-dimensional (2-D) MHD.

In this Letter, we show that, by the addition of a second shell to a shell-on-target gas-puff, the required B_{z0} for MRTI
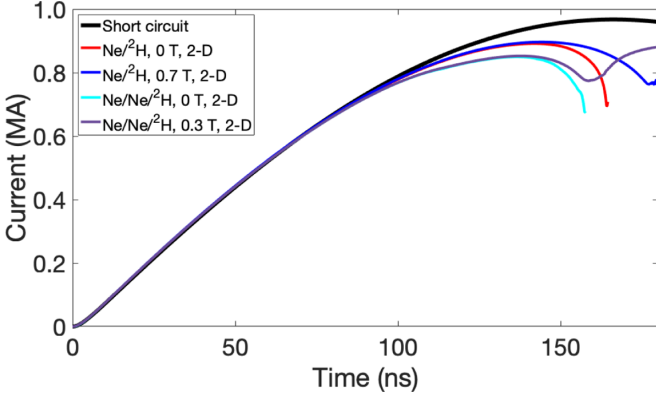
---
*jnarkis@ucsd.edu

FIG. 1. Current traces from HYDRA for the single-liner and double-liner cases with and without B_{z0}, with a trace from a 2.5-cm radius, 1.0-cm length short circuit in black for reference. MRTI growth tends to result in an earlier implosion and a larger inductive dip.

FIG. 2. The estimated number of MRTI e foldings for the single-liner (a) and double-liner (b) simulations with different initial axial magnetic fields as a function of MRTI wavelength. Estimates are made from 1-D simulations by invoking Eqs. (1) and (3).

mitigation is reduced by half. As a result, the central target jet can be compressed to higher temperature and density. To show this, we consider mitigation of 2-D MRTI growth of a neon annular liner of radius 2.5 cm, length 1 cm, with a Gaussian profile with full width at half maximum (FWHM) 0.5 cm, and peak initial density $n_{i0,\text{peak}}$ 3.0×10^{16} cm^{-3} imploding onto an on-axis deuterium target with a Gaussian profile of FWHM 1 cm and $n_{i0,\text{peak}}$ 3.0×10^{17} cm^{-3} using the HYDRA [27] radiation-MHD code. We show that the addition of a second neon liner at radius 1.25 cm, also with a Gaussian profile with FWHM 0.5 cm and $n_{i0,\text{peak}}$ 3.0×10^{16} cm^{-3} (while lowering $n_{i0,\text{peak}}$ of the outer liner by 50% to keep total mass constant) reduces the required B_{z0} for adequate stability from 0.7 T to 0.3 T. The interfaces between the inner liner and target and outer liner and inner liner are at 0.785 cm and 1.9 cm, respectively. When a single liner is used, the same Gaussian profile for the target is used, but a constant fill of 1.5×10^{16} cm^{-3} deuterium is used instead of an "inner liner." This raises the target mass from 0.9 μg/cm to 1.4 μg/cm, which will affect the stagnation conditions and neutron yield, but not MRTI growth because it is a small fraction of the total load mass. To evaluate the effectiveness of MRTI mitigation in the context of neutron yield, we show that the thermonuclear neutron yield obtained in inherently stable 1-D simulations is reproduced in 2-D simulations when a double-liner is used. Note that instability growth in 2-D is seeded by a $\pm 1\%$ random density perturbation, and for brevity, henceforth "Ne/^{2}H" and "Ne/Ne/^{2}H" will refer to the single neon liner on deuterium target and neon-neon double liner on deuterium target configurations, respectively.

The load is driven by the CESZAR [28] linear transformer driver (LTD) charged to ± 100 kV, delivering 850–900 kA to a short-circuit load with rise time 160 ns. There is variability in peak current and rise time for an imploding load due to its large dynamic inductance relative to the driver; the current traces for the presented simulations are shown in Fig. 1 along with a reference current trace with a 2.5-cm-radius, 1-cm-length short circuit load.

To estimate the effectiveness of B_{z0} in MRTI mitigation from a 1-D simulation, we can calculate an instantaneous
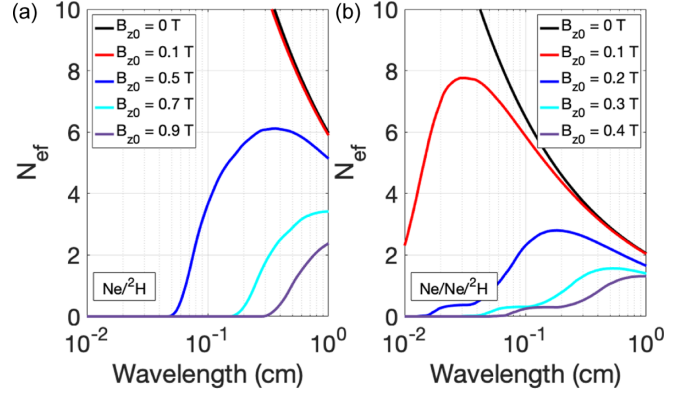
growth rate on the outer liner surface as a function of wavelength using appropriate values of $g(t)$, $B_z(t)$, $n_i(t)$, and the small-curvature approximation of $\gamma(t)$ [Eq. (1)], and make the Wentzel-Kramers-Brillouin-like approximation for the number of e foldings [10]

$$N_{ef} = \int_{t_0}^{t_f} \gamma(t)dt, \qquad (3)$$

where t_0 is the effective start time for instability growth and t_f is the time at stagnation. For the single liner $t_0 = 0$, but as will be shown later for modestly premagnetized double liners, $t_0 \approx 25$ ns prior to peak compression since instability amplitudes are effectively reduced to zero when the liners merge. Acceleration is obtained via fourth-order polynomial fits to radius versus time (that is, piecewise for the double liner, enforcing continuity of radius, velocity, and acceleration), where $r(t)$ is defined by the location of the half-maximum of the density, i.e., where $n_i = n_{i,\text{max}}/2$. The representative density value is taken as $n_i(t) \equiv n_i[r(t), t]$, and similarly $B_z(t) \equiv B_z[r(t), t]$.

By scanning B_{z0} values with 1-D simulations as shown in Fig. 2, we see that a smaller B_{z0} is needed when a double liner is used. For the double liner, the predicted maxima for $B_{z0} = 0.2$, 0.3, and 0.4 T were $N_{ef,\text{max}} = 2.8$, 1.6, and 1.3, respectively, whereas for the single liner the predicted maxima for $B_{z0} = 0.5$, 0.7, and 0.9 T were $N_{ef,\text{max}} = 6.1$, 3.4, and 2.4, respectively. This is because the slower-growing long wavelength modes have adequate time to develop with a single liner and their growth is more difficult to mitigate with axial field line tension. Wavelengths approaching the size of the anode-cathode gap of 1 cm are unlikely to develop, so the approach for selecting B_{z0} is completed in an *ad hoc* fashion by selecting $N_{ef,\text{max}} \leqslant 2$ for wavelengths below 3 mm, or $B_{z0} = 0.7$ T for the single liner and $B_{z0} = 0.3$ T for the double liner.

Let us first consider the single-liner simulations. As shown in Fig. 3, without an axial magnetic field, the characteristic MRTI bubble-and-spike structure has developed by 134 ns. Instabilities have begun to feed through the liner (at $z \sim$ 0.6 cm) into the target at 149 ns. From fast-Fourier-transform (FFT) analysis of the radially integrated mass as a function of
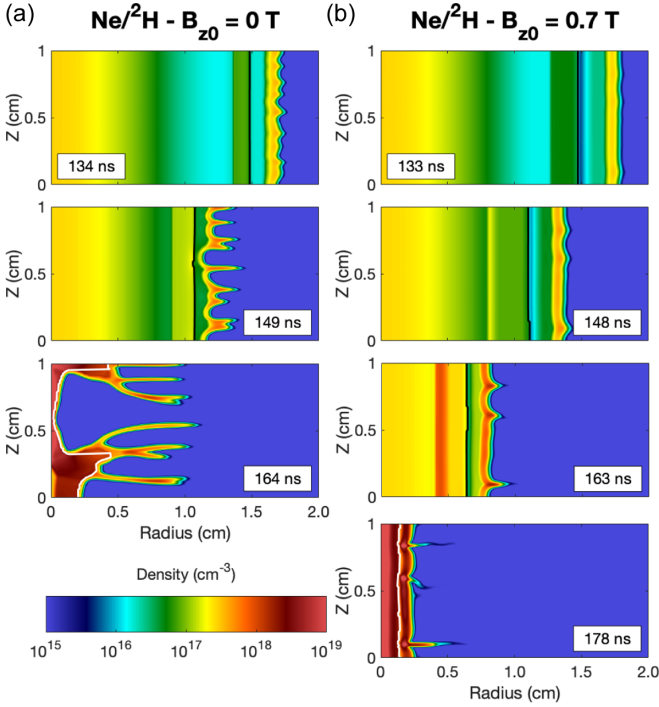
FIG. 3. Ion density contours for the single-liner simulations with $B_{z0} = 0$ T (a) and $B_{z0} = 0.7$ T (b). The contours are taken in 15-ns intervals leading up to the approximate time of peak compression, as defined by axially averaged radius. The interface between the Ne liner and ^{2}H target is denoted by solid black or white lines.

axial position, summarized in Fig. 4, the dominant wavelength of 2 mm continues to grow approximately linearly through ~152 ns, at which point growth saturates and the pinch disassembles. If defined as the time of minimum axially average liner radius, peak compression occurs at 164 ns.

With an applied B_{z0} of 0.7 T, the shorter wavelength modes are suppressed as predicted by the N_{ef} calculations summarized in Fig. 2. Though a clear mode structure has developed by 148 ns, instability amplitude remains low through peak compression. The growth of the dominant mode of 2.5 mm
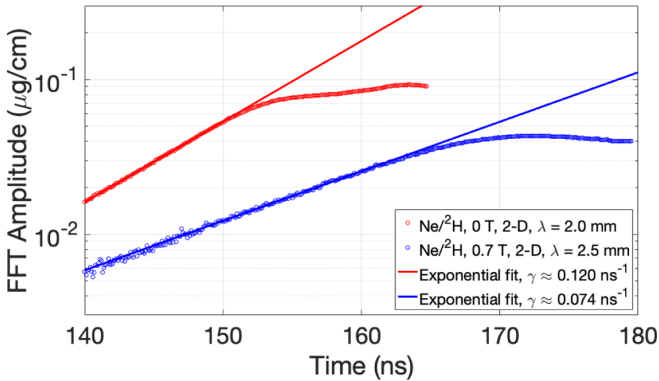

FIG. 4. FFT amplitudes, using radially integrated mass as a function of axial position, of the dominant modes in the single liner cases and exponential fits to windows of approximately linear growth: 140–150 ns for the $B_{z0} = 0$ T case (red) and 150–160 ns for the $B_{z0} = 0.7$ T case (blue).

TABLE I. Average target quantities of interest at peak compression for the single liner implosions and corresponding thermonuclear neutron yield.

	0 T, 1-D	0 T, 2-D	0.7 T, 1-D	0.7 T, 2-D
t [ns]	176.3	164.2	178.8	178.3
r [μm]	302	1954	1135	1326
n_i [cm^{-3}]	6.26×10^{19}	1.02×10^{19}	2.13×10^{19}	1.99×10^{19}
T_i [keV]	8.18	6.35	1.88	1.81
T_e [keV]	2.81	3.48	3.14	2.26
Y_N/cm	8.7×10^9	1.2×10^9	1.2×10^7	1.0×10^7

evolves as shown in Fig. 4. An exponential fit estimates a growth rate of ≈0.074 ns^{-1}, which is lower than the unmagnetized case. More importantly, the pinch column becomes more uniform as it converges at 178 ns; this is seen qualitatively in Fig. 3. While MRTI is mitigated, there is a significant penalty to target compression and neutron yield (two orders of magnitude between the 0 T and 0.7 T simulations) as summarized by the results in Table I. Note that the radius is axially averaged and density and temperature are mass averaged. The most notable result in this table is that the thermonuclear neutron yield is reduced by two orders of magnitude between the 0 T and 0.7 T simulations. The simultaneously large radius and density of the 0 T 2-D simulation reflect the development of instability-driven hot spots.

Turning to the double-liner simulation, mitigation of MRTI is again readily observed by comparing the temporal evolution of density with and without B_{z0}, as shown in Fig. 5. Even without an axial magnetic field MRTI growth is somewhat mitigated by the merging of the inner liner with the outer liner in a process termed "snowplow stabilization" [1,6], resulting in a ~20 ns period of deceleration. Without an axial magnetic field, it can be seen qualitatively in Fig. 5 that instabilities do not grow significantly until snowplow stabilization has ceased. From FFT analysis, summarized in Fig. 6, the amplitude of the dominant 3.3-mm mode remains constant through ~138 ns, after which there is a 10 to 15 ns period of approximately linear growth, at which point the instabilities saturate.

It is apparent from Fig. 5 that the assumption in calculating N_{ef} that instability growth effectively "resets" is not valid for $B_{z0} = 0$ T, but it is valid for $B_{z0} = 0.3$ T. Though the liners merge over the same 110 to 130 ns window as in the $B_{z0} = 0$ case because the magnetic field is not large enough to affect the bulk dynamics, the axial magnetic flux compressed between the two liners provides additional MRTI mitigation beyond that from snowplow stabilization. As in the unmagnetized case, instability growth resumes after the liners have merged, but as with the magnetized single-liner case, its amplitude decreases as the pinch converges.

The primary results of this Letter are summarized in Table II, which compares the Ne/Ne/^{2}H results in one and two dimensions and with $B_{z0} = 0$ T and $B_{z0} = 0.3$ T. Again, note that the radius is axially averaged and density and temperature are mass averaged. Though the stagnation radius increases less from $B_{z0} = 0$ T in one dimension to $B_{z0} = 0$ T in two dimensions with the double liner relative to the single liner, Fig. 5 shows that the pinch is clearly unstable and thus raises questions of reproducibility. However, with the addition
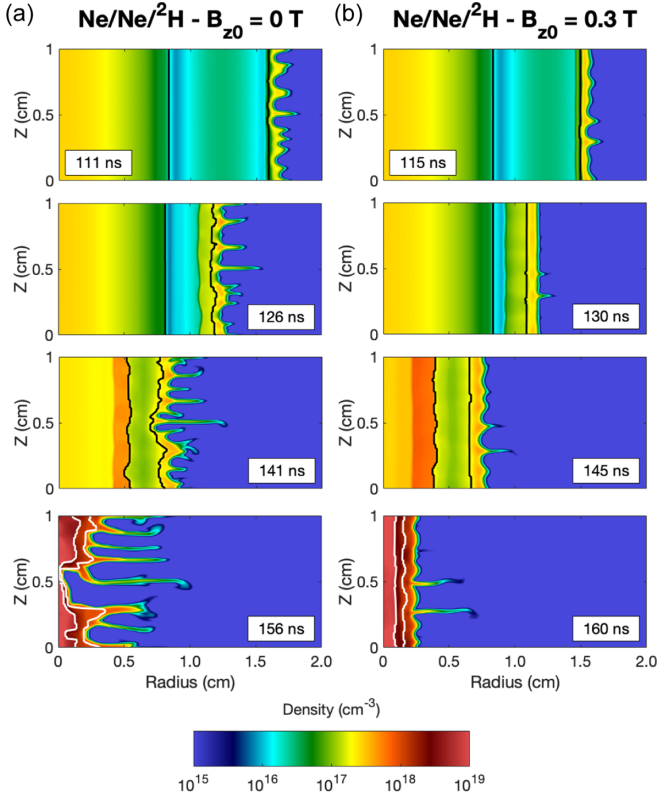
FIG. 5. Ion density contours for the Ne/Ne/^{2}H simulations with $B_{z0} = 0$ T (a) and $B_{z0} = 0.3$ T (b). The contours are taken in 15-ns intervals leading up to the approximate time of peak compression, as defined by axially averaged radius. The interfaces between the inner and outer Ne liners and the Ne liner and ^{2}H target are denoted by solid black or white lines.

of a 0.3 T B_{z0}, the pinch is stabilized and the majority of the yield is recovered in the 2-D simulation relative to the 1-D, $B_{z0} = 0$ T case. This is in stark contrast to the results with a single liner in Table I that predict stabilizing the pinch comes with the tradeoff of a >100× reduction in thermonuclear neutron yield. It is important to note that this may be challenging
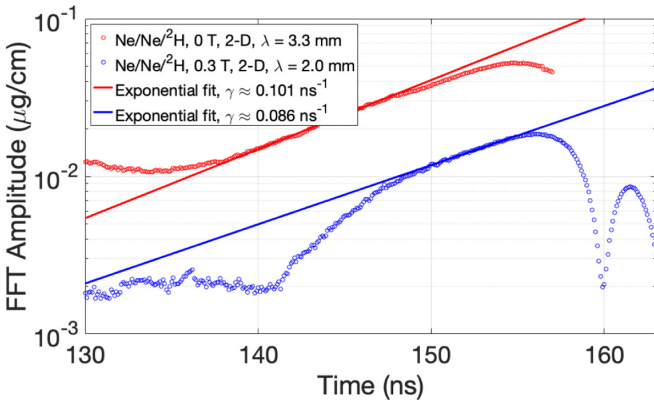

FIG. 6. FFT amplitudes, using radially integrated mass as a function of axial position, of the dominant modes in the double liner case,s and exponential fits to windows of approximately linear growth: 138–148 ns for the $B_{z0} = 0$ T case (red) and 150–155 ns for the $B_{z0} = 0.3$ T case (blue).

TABLE II. Average target quantities of interest at peak compression for the double liner implosions and corresponding neutron yield.

	0 T, 1-D	0 T, 2-D	0.3 T, 1-D	0.3 T, 2-D
t [ns]	159.3	156.5	159.5	160.1
r [μm]	794	832	756	903
n_i [cm^{-3}]	9.50×10^{18}	9.01×10^{18}	1.03×10^{19}	1.02×10^{19}
T_i [keV]	7.39	7.62	6.30	6.47
T_e [keV]	1.33	1.66	1.88	1.48
Y_N/cm	1.6×10^9	1.2×10^9	9.3×10^8	9.8×10^8

to measure experimentally because the beam-target neutron yield can be significant even into the 10-MA range [29,30]. If the beam-target yield is large for the highly unstable unmagnetized pinches, the total neutron yield could actually decrease with B_{z0} by suppressing the beam-target yield in a stabilized pinch. It would potentially be insightful to study this problem with kinetic simulations and/or experiments to investigate potential effects on beam-target neutron yield, which cannot be captured self-consistently in MHD. This could explain, for example, the decrease in neutron yield when B_{z0} is used to stabilize the pinch in recent experiments on the ZEBRA driver [21]. Nevertheless, if this improvement were to hold in future applications on larger drivers, the feasibility of producing a desired neutron flux could increase significantly. Since thermonuclear neutron yield generally scales with the fourth power of driver current [31], a 100 times increase in yield would allow for more than a three times decrease in load current. This is important not only because larger drivers inevitably cost more to construct, operate, and maintain, but also because beyond currents of ~10 MA it is known based on experimental observations [32] that significant hardware damage can occur after each shot, limiting the feasibility of high-repetition-rate operation.

For a peak current of 850 kA and an initial radius of 2.5 cm, values of 0.7 T and 0.3 T correspond to $2.1B_{st}$ and $0.9B_{st}$, respectively, which is higher than what is required from experiments on other drivers [17,18,20,22]. There are multiple possible explanations due to phenomena that cannot be represented in 2-D MHD simulations. One such phenomenon is the partial loss of current drive to a low-density peripheral plasma, in which current may flow force free [20]. A recent computational work using extended-MHD [12] argues that this is a fundamentally 3-D effect with the Hall effect playing a major role. Axial flux amplification and current shunting to the low-density plasma could lower the required imposed B_{z0} to stabilize the pinch significantly.

It is interesting to note for future work that there is a correlation between the ratio of target stagnation T_i/T_e in the presence of B_{z0}. In the regime of university-scale drivers, the dominant energy loss mechanism of the target is electron thermal conduction, rather than radiation [33,34]. The B_{z0} values used for mitigation of MRTI growth also result in substantial thermal insulation; mass-averaged target electron Hall parameters at stagnation for the single liner, 0.7 T B_{z0}, 2-D and double-liner, 0.3 T B_{z0}, 2-D simulations are 5666 and 723, respectively. It will also be shown in future work with scaling studies that the Hall parameter does not remain constant for simulations that enforce comparable dynamics,

which may have implications for the premagnetized triple nozzle concept on multiple and tens of MA drivers. For future design applications, it is important to consider effects that go beyond the scope of this work, including end losses, fuel–liner mixing, and fuel–electrode mixing. Furthermore, radiative losses, electron-ion equilibration, and ion thermal conduction may all become more relevant at higher currents.

[1] J. L. Giuliani and R. J. Commisso, A review of the gas-puff Z-pinch as an X-ray and neutron source, IEEE Trans. Plasma Sci. **43**, 2385 (2015).

[2] D. D. Ryutov, M. S. Derzon, and M. K. Matzen, The physics of fast Z pinches, Rev. Mod. Phys. **72**, 167 (2000).

[3] M. G. Haines, A review of the dense Z-pinch, Plasma Phys. Controlled Fusion **53**, 093001 (2011).

[4] E. G. Harris, Rayleigh-Taylor instabilities of a collapsing cylindrical shell in a magnetic field, Phys. Fluids **5**, 1057 (1962).

[5] A. B. Bud'ko, F. S. Felber, A. I. Kleev, M. A. Liberman, and A. L. Velikovich, Stability analysis of dynamic Z pinches and theta pinches, Phys. Fluids B **1**, 598 (1989).

[6] S. M. Gol'berg and A. L. Velikovich, Suppression of Rayleigh-Taylor instability by the snowplow mechanism, Phys. Fluids B **5**, 1164 (1993).

[7] A. L. Velikovich, F. L. Cochran, and J. Davis, Suppression of Rayleigh-Taylor instability in Z-Pinch loads with tailored density profiles, Phys. Rev. Lett. **77**, 853 (1996).

[8] K. O. Mikaelian, Rayleigh-Taylor and Richtmyer-Meshkov instabilities and mixing in stratified cylindrical shells, Phys. Fluids **17**, 094105 (2005).

[9] M. R. Weis, P. Zhang, Y. Y. Lau, P. F. Schmit, K. J. Peterson, M. Hess, and R. M. Gilgenbach, Coupling of sausage, kink, and magneto-Rayleigh-Taylor instabilities in a cylindrical liner, Phys. Plasmas **22**, 032706 (2015).

[10] A. L. Velikovich and P. F. Schmit, Bell-Plesset effects in Rayleigh-Taylor instability of finite-thickness spherical and cylindrical shells, Phys. Plasmas **22**, 122711 (2015).

[11] P. F. Schmit, A. L. Velikovich, R. D. McBride, and G. K. Robertson, Controlling Rayleigh-Taylor Instabilities in Magnetically Driven Solid Metal Shells by Means of a Dynamic Screw Pinch, Phys. Rev. Lett. **117**, 205001 (2016).

[12] C. E. Seyler, Axial magnetic flux amplification in Hall-magnetohydrodynamic simulations of externally magnetized z-pinches, Phys. Plasmas **27**, 092102 (2020).

[13] D. E. Ruiz, On a variational formulation of the weakly nonlinear magnetic Rayleigh-Taylor instability, Phys. Plasmas **27**, 022121 (2020).

[14] E. Ruden, H. U. Rahman, A. Fisher, and N. Rostoker, Stability enhancement of a low initial density hollow gas-puff z pinch by e- beam preionization, J. Appl. Phys. **61**, 1311 (1987).

[15] F. S. Felber, M. M. Malley, F. J. Wessel, M. K. Matzen, M. A. Palmer, R. B. Spielman, M. A. Liberman, and A. L. Velikovich, Compression of ultrahigh magnetic fields in a gas-puff Z pinch, Phys. Fluids **31**, 2053 (1988).

[16] F. S. Felber, F. J. Wessel, N. C. Wild, H. U. Rahman, A. Fisher, C. M. Fowler, M. A. Liberman, and A. L. Velikovich, Ultrahigh

magnetic fields produced in a gas-puff Z pinch, J. Appl. Phys. **64**, 3831 (1988).

[17] S. Chaikovsky, A. Labetsky, V. Oreshkin, A. Shishlov, R. Baksht, A. Fedunin, and A. Rousskikh, The K-shell radiation of a double gas puff z-pinch with an axial magnetic field, Laser Part. Beams **21**, 255 (2003).

[18] A. V. Shishlov, R. B. Baksht, S. A. Chaikovsky, A. V. Fedunin, F. I. Fursov, V. A. Kokshenev, N. E. Kurmaev, A. Y. Labetsky, V. I. Oreshkin, N. A. Ratakhin *et al.*, Formation of tight plasma pinches and generation of high-power soft X-ray radiation pulses in fast Z-pinch implosions, Laser Phys. **16**, 183 (2006).

[19] D. Mikitchuk, C. Stollberg, R. Doron, E. Kroupp, Y. Maron, H. R. Strauss, A. L. Velikovich, and J. L. Giuliani, Mitigation of instabilities in a Z-pinch plasma by a preembedded axial magnetic field, IEEE Trans. Plasma Sci. **42**, 2524 (2014).

[20] D. Mikitchuk, M. Cvejić, R. Doron, E. Kroupp, C. Stollberg, Y. Maron, A. L. Velikovich, N. D. Ouart, J. L. Giuliani, T. A. Mehlhorn, E. P. Yu, and A. Fruchtman, Effects of a Preembedded Axial Magnetic Field on the Current Distribution in a Z-Pinch Implosion, Phys. Rev. Lett. **122**, 045001 (2019).

[21] H. U. Rahman, E. Ruskov, P. Ney, F. Conti, J. C. Valenzuela, N. Aybar, J. Narkis, F. N. Beg, E. Dutra, and A. Covington, Ar and Kr on deuterium gas-puff staged Z-pinch implosions on a 1-MA driver: experiment and simulation, Phys. Plasmas **26**, 052706 (2019).

[22] F. Conti, N. Aybar, J. Narkis, J. C. Valenzuela, H. U. Rahman, E. Ruskov, E. Dutra, S. Haque, A. Covington, and F. N. Beg, Study of stability in a liner-on-target gas puff Z-pinch as a function of pre-embedded axial magnetic field, Phys. Plasmas **27**, 012702 (2020).

[23] E. S. Lavine, S. V. Rocco, J. T. Banasek, W. M. Potter, J. B. Greenly, H. Wilhelm, N. Qi, D. A. Hammer, and B. R. Kusse, Implosion dynamics of triple-nozzle gas-puff z pinches on CO-BRA, Phys. Plasmas **28**, 022703 (2021).

[24] T. J. Awe, R. D. McBride, C. A. Jennings, D. C. Lamppa, M. R. Martin, D. C. Rovang, S. A. Slutz, M. E. Cuneo, A. C. Owen, D. B. Sinars *et al.*, Observations of Modified Three-Dimensional Instability Structure for Imploding Z-Pinch Liners that are Premagnetized with An Axial Field, Phys. Rev. Lett. **111**, 235005 (2013).

[25] C. A. Coverdale, C. Deeney, A. L. Velikovich, R. W. Clark, Y. K. Chong, J. Davis, J. Chittenden, C. L. Ruiz, G. W. Cooper, A. J. Nelson *et al.*, Neutron production and implosion characteristics of a deuterium gas-puff Z pinch, Phys. Plasmas **14**, 022706 (2007).

[26] S. A. Slutz, M. C. Herrmann, R. A. Vesey, A. B. Sefkow, D. B. Sinars, D. C. Rovang, K. J. Peterson, and M. E. Cuneo,

Pulsed-power-driven cylindrical liner implosions of laser pre-heated fuel magnetized with an axial field, Phys. Plasmas **17**, 056303 (2010).

[27] M. M. Marinak, G. D. Kerbel, N. A. Gentile, O. Jones, D. Munro, S. Pollaine, T. R. Dittrich, and S. W. Haan, Three-dimensional HYDRA simulations of National Ignition Facility targets, Phys. Plasmas **8**, 2275 (2001).

[28] F. Conti, J. C. Valenzuela, V. Fadeev, N. Aybar, D. B. Reisman, A. Williams, G. Collins, J. Narkis, M. P. Ross, F. N. Beg *et al.*, MA-class linear transformer driver for Z-pinch research, Phys. Rev. Accel. Beams **23**, 090401 (2020).

[29] D. R. Welch, D. V. Rose, R. E. Clark, C. B. Mostrom, W. A. Stygar, and R. J. Leeper, Fully Kinetic Particle-in-Cell Simulations of a Deuterium gas Puff z Pinch, Phys. Rev. Lett. **103**, 255002 (2009).

[30] D. R. Welch, D. V. Rose, C. Thoma, R. E. Clark, C. B. Mostrom, W. A. Stygar, and R. J. Leeper, Kinetic simulation

of thermonuclear-neutron production by a 10^7-A deuterium Z pinch, Phys. Plasmas **17**, 072702 (2010).

[31] A. L. Velikovich, R. W. Clark, J. Davis, Y. K. Chong, C. Deeney, C. A. Coverdale, C. L. Ruiz, G. W. Cooper, A. J. Nelson, J. Franklin *et al.*, Z-pinch plasma neutron sources, Phys. Plasmas **14**, 022701 (2007).

[32] R. Spielman, D. Froula, G. Brent, E. Campbell, D. Reisman, M. Savage, M. Shoup, W. Stygar, and M. Wisher, Conceptual design of a 15-TW pulsed-power accelerator for high-energy-density-physics experiments, Matter Radiat. Extremes **2**, 204 (2017).

[33] I. R. Lindemuth, The ignition design space of magnetized target fusion, Phys. Plasmas **22**, 122712 (2015).

[34] J. Narkis, H. U. Rahman, J. C. Valenzuela, F. Conti, R. D. McBride, D. Venosa, and F. N. Beg, A semi-analytic model of gas-puff liner-on-target magneto-inertial fusion, Phys. Plasmas **26**, 032708 (2019).